
Unsupervised Evolutionary Cell Type Matching via Entropy-Minimized Optimal Transport

Mu Qiao
muqiao0626@gmail.com

Abstract

Identifying evolutionary correspondences between cell types across species is a fundamental challenge in comparative genomics and evolutionary biology. Existing approaches often rely on either reference-based matching, which imposes asymmetry by designating one species as the reference, or projection-based matching, which may increase computational complexity and obscure biological interpretability at the cell-type level. Here, we present OT-MESH, an unsupervised computational framework leveraging entropy-regularized optimal transport (OT) to systematically determine cross-species cell type homologies. Our method uniquely integrates the Minimize Entropy of Sinkhorn (MESH) technique to refine the OT plan. It begins by selecting genes with high Signal-to-Noise Ratio (SNR) to capture the most informative features, from which a cost matrix is constructed using cosine distances between cell-type centroids. Importantly, the MESH procedure iteratively refines the cost matrix, leading to a transport plan with significantly enhanced sparsity and interpretability of the resulting correspondence matrices. Applied to retinal bipolar cells (BCs) and retinal ganglion cells (RGCs) from mouse and macaque, OT-MESH accurately recovers known evolutionary relationships and uncovers novel correspondences, one of which was independently validated experimentally. Thus, our framework offers a principled, scalable, symmetric, and interpretable solution for evolutionary cell type mapping, facilitating deeper insights into cellular specialization and conservation across species.

1 Introduction

Understanding evolutionary relationships between cell types across species is central to elucidating mechanisms underlying cellular specialization and diversity. Recent advances in single-cell RNA sequencing (scRNA-seq) have greatly improved the characterization of cell types based on their gene expression profiles across diverse species [1, 2]. However, a fundamental challenge persists: given independently identified clusters of transcriptionally similar cells from different species, how can we systematically and reliably determine their evolutionary correspondences?

Existing methods for cross-species cell type alignment broadly fall into two categories [3]: (1) reference-based matching, in which classifiers are trained on labeled data from a reference species to predict cell types in a query species [4, 5, 6, 7]; and (2) projection-based matching, in which individual-cell gene expression profiles from different species are embedded into a shared low-dimensional space using algorithms such as Canonical Correlation Analysis (CCA), Harmony, or other manifold alignment techniques [8, 9, 10]. Reference-based matching inherently introduces asymmetry by designating one species as the "reference" and the other as the "query," potentially biasing outcomes, especially when species differ significantly in cell type numbers or evolutionary distances. Projection-based matching, though symmetric, typically operates at the level of individual cells, resulting in high computational demands and potentially obscuring direct biological interpretability of cell-type level relationships. Alternatively, cell type correspondences have been inferred through expert-curated morphological, physiological, or marker-gene criteria [2, 11]. While valuable, these expert-driven methods depend heavily on prior hypotheses and manual validations, limiting scalability and systematic applicability.

To address these limitations, we introduce OT-MESH, an unsupervised computational framework. It combines entropy-regularized optimal transport (OT), a powerful tool for comparing distributions and finding correspondences, with a novel integration of the Minimize Entropy of Sinkhorn (MESH) refinement strategy [12]. OT is well-suited for this task due to its inherent ability to handle asymmetric numbers of types and partial correspondences. However, standard entropy-regularized OT often yields diffuse, non-sparse transport plans, hindering direct biological interpretation. Inspired by developments in machine learning and computer vision [13, 14], we adapt the MESH technique to iteratively refine the OT cost matrix, promoting sparsity in the cross-species cell type alignment. Our method begins with Signal-to-Noise Ratio (SNR) based gene selection to identify informative features. It then constructs a cost matrix from cosine distances between cell-type centroids in this selected gene space. The MESH procedure is subsequently applied to refine the transport plan, yielding sparse and interpretable correspondence matrices.

We illustrate our approach using established datasets of bipolar cells (BCs) and retinal ganglion cells (RGCs) from mouse and macaque retinas [2, 5, 15]. Leveraging existing knowledge for validation, we demonstrate that our method consistently identifies known evolutionary correspondences and discovers novel cell-type homologies, including one correspondence independently validated experimentally [16]. Thus, OT-MESH provides a principled, scalable, and interpretable computational framework, enhancing our ability to map cell type evolution and advance its understanding.

2 Background

2.1 Optimal Transport (OT) for Correspondence Problems

OT provides a principled mathematical framework for identifying correspondence between distributions. Given two distributions supported on spaces \mathbf{X} and \mathbf{Y} , OT seeks the optimal mapping that minimizes the total cost of transporting mass from \mathbf{X} to \mathbf{Y} . In discrete form, it involves finding a transport plan \mathbf{W} that minimizes

$$L(\mathbf{W}) = \sum_{ij} W_{ij} C_{ij}, \quad (1)$$

where C_{ij} is the cost of transporting unit mass from point i in \mathbf{X} to point j in \mathbf{Y} .

To enhance computational tractability and numerical stability, OT problems often incorporate entropy regularization, which encourages smoother transport plans. The entropy-regularized OT problem is formulated as:

$$L(\mathbf{W}) = \sum_{ij} W_{ij} C_{ij} + \alpha \sum_{ij} W_{ij} (\log W_{ij} - 1), \quad (2)$$

subject to the marginal constraints:

$$\sum_j W_{ij} = p_i, \quad \sum_i W_{ij} = q_j. \quad (3)$$

Here, p_i and q_j define prescribed marginals. This entropy-regularized problem can be efficiently solved using the Sinkhorn algorithm [17].

2.1.1 Sinkhorn Algorithm

Given a cost matrix $\mathbf{C} \in \mathbb{R}^{a \times b}$, a regularization parameter $\alpha > 0$, and prescribed marginal distributions $\mathbf{p} \in \mathbb{R}^a$ and $\mathbf{q} \in \mathbb{R}^b$, the Sinkhorn algorithm computes the Gibbs kernel as:

$$\mathbf{G} = \exp \left(-\frac{\mathbf{C}}{\alpha} \right). \quad (4)$$

It iteratively updates two scaling vectors \mathbf{u} and \mathbf{v} as follows:

$$\mathbf{u} \leftarrow \mathbf{p} \oslash (\mathbf{G}\mathbf{v}), \quad \mathbf{v} \leftarrow \mathbf{q} \oslash (\mathbf{G}^\top \mathbf{u}), \quad (5)$$

where \oslash denotes element-wise division. After convergence, the final transport matrix is obtained by:

$$\mathbf{W} = \text{diag}(\mathbf{u}) \mathbf{G} \text{diag}(\mathbf{v}). \quad (6)$$

In practice, computations are frequently performed in log-space to maintain numerical stability.

2.2 Minimize Entropy of Sinkhorn (MESH)

While entropy regularization makes OT computationally tractable, it often produces overly diffuse (low interpretability) transport plans with limited interpretability, especially when the underlying biological correspondences are expected to be sparse. To address this, the MESH approach [12] iteratively refines the cost matrix itself to minimize the entropy of the resulting transport plan:

$$\mathbf{C}'(t+1) = \mathbf{C}'(t) - \lambda \frac{\nabla_{\mathbf{C}'(t)} H(\text{sinkhorn}(\mathbf{C}'(t)))}{\|\nabla_{\mathbf{C}'(t)} H(\text{sinkhorn}(\mathbf{C}'(t)))\|}, \quad (7)$$

where the entropy of the transport plan $\mathbf{W}(t) = \text{sinkhorn}(\mathbf{C}'(t))$ is defined as:

$$H(\mathbf{W}(t)) = - \sum_{ij} W_{ij}(t) \log W_{ij}(t), \quad (8)$$

and λ is a learning rate. This iterative approach yields sparse and interpretable correspondence matrices by concentrating mass onto fewer, more meaningful connections.

2.3 OT Applications in Single-Cell Biology

OT methods have found increasing applications in single-cell biology, particularly for aligning cell states across experimental conditions, measurement modalities, or developmental time points [18, 19, 20]. A key advantage of OT approaches lies in their natural ability to handle partial or incomplete correspondences. Recent studies have leveraged OT to construct hierarchical cell-type taxonomies, effectively identifying cell types uniquely represented in specific datasets [20]. Nonetheless, OT-based methods have yet to be comprehensively developed and validated specifically for cross-species evolutionary cell type comparisons. In this study, we address this critical gap by adapting and extending OT methodologies, particularly through the MESH procedure, to the problem of cross-species cell type matching.

3 Methods

3.1 Problem Formulation

We consider two species containing a and b distinct cell types, indexed by i and j respectively. For the i th cell type in the first species, let $\mathbf{x}_{ik} \in \mathbb{R}^{1 \times g}$ represent the gene expression vector of the k th cell; similarly, let $\mathbf{y}_{jl} \in \mathbb{R}^{1 \times g}$ denote expression for the l th cell of the j th type in the second species. Our goal is to identify an optimal correspondence matrix $\mathbf{W} \in \mathbb{R}^{a \times b}$ where each element W_{ij} assigns a probability to each pair of cell types being evolutionarily related.

3.2 Gene Selection by Signal-to-Noise Ratio (SNR)

Rather than using all available genes, which can introduce noise and increase computational burden, we identify a subset of highly informative genes based on their expression SNR [2]. SNR prioritizes genes that show high variance between cell types relative to variance within cell types, thus highlighting genes that effectively distinguish types. Specifically, for each gene g , intra-type variances $s_{i,g}^2$ and $s_{j,g}^2$ are computed as:

$$s_{i,g}^2 = \frac{\sum_k (x_{ik,g} - \bar{x}_{i:,g})^2}{n_i}, \quad s_{j,g}^2 = \frac{\sum_l (y_{jl,g} - \bar{y}_{j:,g})^2}{n_j}. \quad (9)$$

where $\bar{x}_{i:,g}$ and $\bar{y}_{j:,g}$ denote the mean expression level of gene g for cell types i and j respectively, and n_i, n_j represent the numbers of cells in those types. The SNR for each gene g is calculated by:

$$\text{SNR}(g) = \frac{\text{Var}(\{\bar{x}_{1:,g}, \dots, \bar{x}_{a:,g}, \bar{y}_{1:,g}, \dots, \bar{y}_{b:,g}\})}{\frac{1}{a+b} \left(\sum_{i=1}^a s_{i,g}^2 + \sum_{j=1}^b s_{j,g}^2 \right)}. \quad (10)$$

We retain genes exceeding a predefined SNR threshold, resulting in m selected genes used to construct the centroid matrices $\hat{\mathbf{X}} \in \mathbb{R}^{a \times m}$ for the first species, and $\hat{\mathbf{Y}} \in \mathbb{R}^{b \times m}$ for the second species.

3.3 Cost Matrix Construction

We define a scale-invariant cost matrix $\mathbf{C} \in \mathbb{R}^{a \times b}$ based on the cosine distance between cell-type centroids:

$$C_{ij} = 1 - \frac{\hat{\mathbf{X}}_i \cdot \hat{\mathbf{Y}}_j}{\|\hat{\mathbf{X}}_i\| \|\hat{\mathbf{Y}}_j\|}. \quad (11)$$

Here, $\hat{\mathbf{X}}_i$ and $\hat{\mathbf{Y}}_j$ are the centroid vectors of cell types i and j respectively.

3.4 Entropy-Regularized OT with MESH

To obtain sparse and interpretable correspondences, we employ entropy-regularized OT refined by the MESH procedure. We begin with a slightly perturbed initial cost matrix [12]:

$$\mathbf{C}'(0) = \mathbf{C} + \varepsilon, \quad \varepsilon_{ij} \sim \mathcal{N}(0, 10^{-6}), \quad (12)$$

At each iteration t , we compute the transport plan $\mathbf{W}(t)$ from the current cost matrix $\mathbf{C}'(t)$ using the Sinkhorn algorithm and then quantify its entropy:

$$F(\mathbf{C}'(t)) = H(\mathbf{W}(t)) = - \sum_{ij} W_{ij}(t) \log W_{ij}(t). \quad (13)$$

The cost matrix is updated by gradient descent, normalized to maintain stable updates:

$$\mathbf{C}'(t+1) = \mathbf{C}'(t) - \lambda \frac{\nabla_{\mathbf{C}'(t)} F(\mathbf{C}'(t))}{\|\nabla_{\mathbf{C}'(t)} F(\mathbf{C}'(t))\|}, \quad (14)$$

After T iterations, the resulting cost matrix $\mathbf{C}'(T)$ is used to compute the final transport plan:

$$\mathbf{W}^* = \text{sinkhorn}(\mathbf{C}'(T)). \quad (15)$$

3.5 Algorithm Summary

Our entire approach is summarized as Algorithm 1 and illustrated schematically in Figure 1.

Algorithm 1 Evolutionary Cell Type Matching via Entropy-Regularized OT with MESH

- 1: **Input:** Centroid matrices from SNR-selected genes, $\hat{\mathbf{X}} \in \mathbb{R}^{a \times m}$ and $\hat{\mathbf{Y}} \in \mathbb{R}^{b \times m}$, regularization parameter α , MESH learning rate λ , number of MESH iterations T
 - 2: Compute cost matrix $\mathbf{C} \in \mathbb{R}^{a \times b}$ as in Eq. 11
 - 3: Initialize marginal distributions \mathbf{p} , \mathbf{q} , and $\mathbf{C}'(0)$ as in Eq. 12
 - 4: For $t = 0$ to $T - 1$:
 - 5: Compute $\mathbf{W}(t) = \text{sinkhorn}(\mathbf{C}'(t))$
 - 6: Calculate entropy $F(\mathbf{C}'(t))$ as in Eq. 13
 - 7: Update $\mathbf{C}'(t+1)$ using Eq. 14
 - 8: **Output:** Final correspondence matrix \mathbf{W}^* as in Eq. 15
-

4 Experimental Setup

4.1 Datasets

We evaluated our method using three established retinal cell datasets:

- Macaque BC and RGC data from peripheral or foveal retina reported by Peng et al. [5].
- Mouse BC dataset from Shekhar et al. [4].
- Mouse RGC dataset from Tran et al. [15].

We first validated our method on macaque retinal BC types with known correspondences between peripheral and foveal regions. Specifically, we created a ground-truth test case comprising 12 BC types with exact 1:1 matching across these regions (excluding the fovea-specific "OFFx" type). Subsequently, we extended our analyses to cross-species comparisons: mouse BC (15 types) versus macaque BC (12 types), and mouse RGC (45 types) versus macaque foveal RGC (18 types).

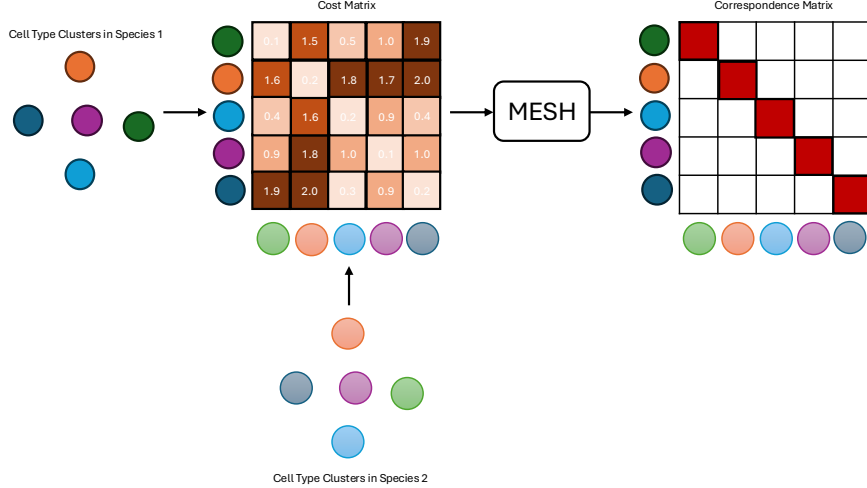


Figure 1: Illustration of the proposed method. Cell type centroids are computed using SNR-selected genes, and a cost matrix is constructed using cosine distance between these centroids for the first and second species. The MESH procedure iteratively refines this cost matrix to produce the final correspondence matrix that reveals evolutionarily related cell types with sparse, interpretable mappings that quantify the strength of relationships between cell types across species.

4.2 Preprocessing and Feature Selection

We adhered to previously established preprocessing and feature selection protocols [2, 4, 5, 15, 21, 22]. Orthologous genes between mouse and macaque were identified using standard orthology databases, resulting in 10,416 common genes. Cell transcript counts were normalized to the median total transcript count per cell, followed by log-transformation to stabilize variance and mitigate technical variability.

For feature selection, we ranked genes by their SNR (Eq. 10) and retained genes surpassing an empirical threshold ($\text{SNR} > 100$, yielding a manageable number of highly discriminative genes, typically a few hundred to a thousand in our datasets), resulting in a subset of genes that effectively differentiate cell types. Cell-type centroids were computed based on these selected genes, forming input matrices $\hat{\mathbf{X}}$ and $\hat{\mathbf{Y}}$ to the OT algorithm.

4.3 Cell Type Correspondence

We formulated cell type correspondence as an OT problem with uniform marginals, $p_i = 1/a$ and $q_j = 1/b$. This choice reflects an agnostic prior about correspondences and prevents dominant cell types from disproportionately influencing the correspondence matrix.

To quantify correspondence strength between cell types between cell types i, j from the final transport matrix \mathbf{W}^* , we defined an alignment score s_{ij} as:

$$s_{ij} = \frac{1}{2} \left(\frac{W_{ij}^*}{\sum_{k=1}^a W_{kj}^*} + \frac{W_{ij}^*}{\sum_{l=1}^b W_{il}^*} \right). \quad (16)$$

This score s_{ij} represents the average of two probabilities: the probability of cell type i in species one matching type j among all cell types in species two, and vice versa. By averaging both row-wise and column-wise normalized weights, this metric robustly identifies and ranks strong bidirectional evolutionary relationships.

For interpretation of cross-species RGC correspondences, we integrated established morphological and functional annotations from prior comprehensive studies [22, 23]. This allowed mapping of transcriptomic clusters from the mouse dataset [15] to functionally characterized RGC subtypes, such as alpha, direction-selective, and intrinsically photosensitive RGCs, thereby facilitating biological interpretation of identified macaque RGC counterparts.

4.3.1 Evaluation Metrics

We used four key metrics to assess our approach:

- Sparseness Score: Proportion of negligible entries (<0.001) in the correspondence matrix, indicating interpretability through sparsity.
- Entropy: Quantifies uncertainty or diffuseness of correspondence assignments (Eq. 13); lower entropy indicates clearer correspondences.
- Adjusted Rand Index (ARI): Measures agreement between predicted correspondences and known ground-truth assignments; higher ARI indicates greater accuracy.
- Running Time: Computational efficiency measured by elapsed processing time.

4.3.2 Parameter Selection

We conducted systematic parameter optimization through grid search over the following parameter ranges:

- Regularization parameter α : [0.01, 0.1, 1.0, 10.0]
- MESH learning rate λ : [0.1, 0.5, 1.0, 5.0]
- Number of MESH iterations T : [1.0, 2.0, 4.0, 8.0]

For each parameter combination, we computed the transport loss (Eq. 2) and sparseness score. Because our primary aim was sparse and interpretable correspondences, we restricted our selection to parameter sets with sparseness scores above 0.5, choosing the set that minimized transport loss. Optimal parameters were independently determined for each experiment, detailed in Supplementary-Figures 1–3.

4.3.3 Comparative Baselines

To contextualize our method, we compared it against three baseline approaches:

- XGBoost classification (reference-based matching): A supervised classification approach commonly used in previous cross-species studies [5, 6, 7]. An XGBoost classifier is trained on cell types from a designated reference species using orthologous gene expression profiles, and applied to predict cell types in a query species. The correspondence matrix is derived by aggregating the predicted labels of individual query cells to quantify cell-type level relationships.
- Harmony integration followed by 1-Nearest Neighbor (Harmony+1NN, projection-based matching): Harmony [9] integrates individual-cell transcriptomic profiles from different species into a shared low-dimensional embedding, correcting batch effects. Cell-type correspondences are inferred by assigning each cell to the cell type of its nearest neighbor from the other species in the integrated space. These individual-level assignments are then aggregated to form a correspondence matrix reflecting inter-species cell-type alignments.
- Entropy-regularized OT without MESH refinement: To explicitly evaluate the benefit of MESH, we included standard entropy-regularized OT as a baseline, using the same SNR-selected genes for fair comparison.

All methods were evaluated using the previously described metrics, allowing rigorous comparison of accuracy, interpretability, and computational efficiency.

5 Results

5.1 Method Validation and Comparison

We first validated our OT-MESH method against known cell type correspondences between macaque peripheral and foveal bipolar cells (BCs), comparing its performance to three baseline methods: XGBoost, Harmony+1NN, and standard entropy-regularized OT without MESH. For XGBoost, the classifier was trained using macaque foveal BCs as the reference [5]. For Harmony+1NN, we performed embedding based integration followed by cell type label transfer through nearest neighbor

assignment in the harmonized PCA space [9]. Standard OT was performed using the same parameters as OT-MESH but without iterative entropy minimization.

Figure 2 illustrates the resulting correspondence matrices. The XGBoost approach (Figure 2A) yielded a predominantly diagonal structure with notable off-diagonal noise. Harmony+INN (Figure 2B) improved upon XGBoost by producing cleaner correspondences, though some off-diagonal elements persisted. Standard OT without MESH refinement (Figure 2C) produced a highly diffuse correspondence matrix, making interpretation nearly impossible despite its computational speed. In contrast, OT-MESH (Figure 2D) resulted in a clean diagonal structure with high-confidence values, clearly recovering the true 1:1 correspondences.

Quantitative metrics (Table 1) reinforce these findings. OT-MESH achieved the best overall performance: highest sparseness (0.8678), lowest entropy (2.4597), and highest ARI (0.9779). Harmony+INN was second in sparseness (0.8347) and ARI (0.9258) but was significantly slower (14.5306s vs. 0.7626s for OT-MESH). XGBoost had lower ARI (0.8871) and was slower than OT-MESH (2.3062s). Standard OT was fastest (0.0329s) but its extremely low sparseness (0), poor ARI (0.0240), and diffuse nature made it unsuitable for meaningful biological interpretation. These results demonstrate that OT-MESH provides a compelling balance of accuracy, interpretability, and computational efficiency for cross-species cell type correspondence.

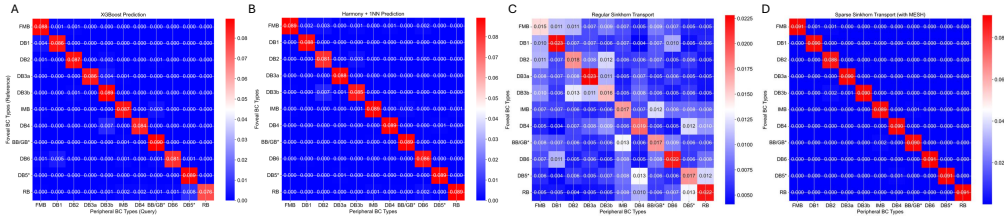


Figure 2: Comparison of correspondence matrices for macaque peripheral to foveal BC type mapping. A) XGBoost shows diagonal structure but with some off-diagonal noise. B) Harmony+INN improves alignment with cleaner structure. C) Regular OT produces a diffuse, uninterpretable mapping. D) OT-MESH yields the clearest diagonal structure with high-confidence 1:1 matchings, consistent with ground truth. Correspondence matrices are normalized so that the sum of all their entries is one.

Table 1: Performance comparison of cross-species cell type matching methods on macaque foveal vs. peripheral BC types. Best values for each metric are in bold.

Method	Sparseness Score	Entropy	ARI	Running Time (s)
XGBoost	0.8017	2.6738	0.8871	2.3062
Harmony+INN	0.8347	2.5949	0.9258	14.5306
OT without MESH	0.0000	4.6934	0.0240	0.0329
OT-MESH	0.8678	2.4597	0.9779	0.7626

5.2 Cross-Species Correspondence of Bipolar Cell (BC) Types

We next applied OT-MESH to cross-species alignment of BC types between mouse (15 types) and macaque (12 types). The resulting correspondence matrix (Figure 3A) reveals clear evolutionary matches, forming strong diagonal-like patterns.

Alignment scores (SupplementaryTable 1) quantify these correspondences. The strongest match was between mouse RBC and macaque RB (rod BCs), with a score of 0.91. Among cone BCs, macaque DB1, DB2, DB3a, DB3b, DB6, IMB, and BB/GB* types were uniquely and strongly assigned to mouse BC2, BC4, BC3A, BC3B, BC6, BC7, and BC8/9 types, respectively, consistent with previous reports [2, 4].

The remaining three macaque BC types showed more complex mappings. Macaque FMB corresponded to both mouse BC1A and BC1B. Macaque DB4 mapped to both mouse BC5A and BC5D. Notably, macaque DB5* showed distributed correspondence with mouse BC5B and BC5C. The mapping of DB5* (a cone BC) to mouse BC5B/C (cone BCs) is more consistent with their shared functional (ON pathway) and morphological (axon terminal stratification in middle IPL) properties

[24, 25] compared with a previous report mapping it to mouse RBC (a rod BC) [4]. This highlights OT-MESH’s ability to uncover complex homologies.

5.3 Cross-Species Correspondence of Ganglion Cell (RGC) Types

When applied to the more complex case of RGC types (45 mouse types vs. 18 macaque foveal types), OT-MESH successfully recovered meaningful cross-species correspondences despite the substantial difference in type numbers and greater evolutionary divergence. Figure 3B visualizes these relationships, showing a sparser correspondence matrix compared to BCs, but with several strong matches between functionally similar types, reflecting known conserved pathways and also specialized lineages.

Most notably, our analysis confirmed the correspondence between mouse alpha RGCs and primate midget/parasol ganglion cells with high confidence (SupplementaryTable 2). Specifically, mouse OFF transient alpha (C45) maps strongly to macaque OFF parasol ganglion cells (PG-OFF) (score: 0.61), while ON sustained alpha (C43) corresponds to macaque ON midget ganglion cells (MG-ON) (score: 0.52). Similarly, mouse ON transient alpha (C41) and OFF sustained alpha (C42) map to macaque ON parasol (PG-ON) and OFF midget ganglion cells (MG-OFF) respectively (scores: 0.23 and 0.20). This provides additional support for the evolutionary relationship between these cell types, consistent with the recent report [2]. The correspondence is particularly compelling as it respects both response polarity (ON vs. OFF) and kinetics (sustained vs. transient), suggesting conservation of fundamental visual processing channels across mammalian evolution.

Importantly, OT-MESH identified the strongest overall correspondence between macaque fRGC12 and mouse type C10 (an ON direction-selective RGC) with a high alignment score of 0.66 (SupplementaryTable 2). This finding suggests a previously underappreciated evolutionary relationship between these types. Notably, the existence of an ON direction-selective RGC in primate retina was independently confirmed by Wang et al. [16], lending strong external validation to our method’s predictive power. We also detected robust correspondences between macaque fRGC14 and mouse melanopsin-expressing ipRGCs (C40 and C33, corresponding to M1 subtypes) (scores: 0.60 and 0.40), confirming the conservation of this non-image-forming visual pathway across mammals; and the mapping between macaque fRGC11 and mouse F-mini-ON cells (C3) (score: 0.22), suggesting potential evolutionary links between these functionally specialized types. The correspondence matrix also revealed that many mouse RGC types lacked clear macaque counterparts, suggesting evolutionary specialization in the murine lineage.

Collectively, these results illustrate that OT-MESH captures both well-known and novel cross-species relationships among RGCs. The increased complexity and divergence in RGC mappings, relative to BCs, align with expectations for output neurons under greater evolutionary selection pressure [2, 5].

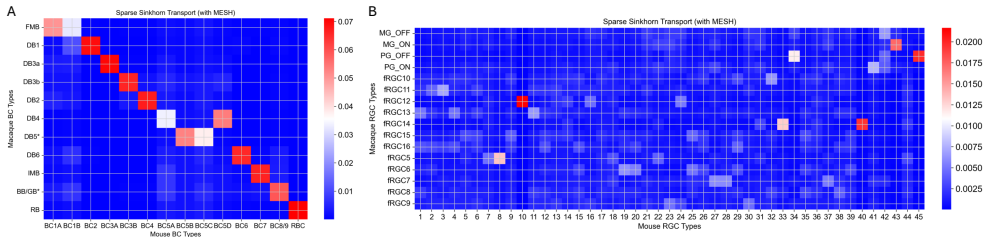


Figure 3: Cross-species correspondence matrices. A) Mouse-to-macaque BC correspondence showing clear mapping between evolutionarily conserved types. B) Mouse-to-macaque RGC correspondence revealing more complex relationships due to the difference in type numbers (45 mouse vs. 18 macaque types).

6 Discussion

We have presented OT-MESH, an unsupervised computational framework that systematically identifies evolutionary correspondences between cell types across species. The core innovation lies in the integration of the MESH procedure with an SNR-based gene selection and centroid-based OT cost matrix. This combination transforms standard OT outputs into sparse and biologically interpretable correspondence matrices. Applied to retinal neuron datasets from mouse and macaque,

OT-MESH successfully recovered known homologies and revealed novel, biologically plausible correspondences. Its ability to quantify alignment strength and robustly handle differences in cell type numbers enhances its utility for cross-species comparative analysis. The observed patterns of conservation (e.g., in BCs) and divergence (e.g., more specialized RGCs in mouse) align with existing biological understanding, while newly predicted matchings offer clear avenues for future experimental validation.

Compared to existing methods, OT-MESH demonstrates several clear advantages. In contrast to reference-based classifiers such as XGBoost [5, 6, 7], OT-MESH is unsupervised and symmetric, requiring no designation of reference versus query species. By operating directly on cell-type centroids rather than individual cells, it achieves significant computational efficiency compared to cell-level projection-based matching methods such as Harmony [9]. Unlike standard entropy-regularized OT, which yields overly diffuse and uninterpretable transport plans, the MESH refinement produces sparse correspondence matrices that align closely with biological intuition and ground truth. This interpretability enables direct hypothesis generation, as exemplified by the high-confidence alignment between macaque fRGC12 and mouse ON direction-selective RGC (C10), which was independently validated by Wang et al. [16]. This finding illustrates how OT-MESH not only recovers known relationships but also predicts new ones with potential biological relevance.

While this study focused on transcriptomic data, our framework is readily extensible. Future versions could incorporate additional modalities, such as epigenomic states, spatial localization, or electrophysiological properties, to more robustly define cell types and resolve ambiguities that transcriptomics alone may not disentangle. Similarly, although SNR-based gene selection and cosine distance proved effective and computationally tractable, alternative feature selection strategies or dissimilarity metrics beyond SNR and cosine distance could also be explored. Beyond the retina, OT-MESH can be applied to explore evolutionary mapping of cell types across other organ systems (e.g., cortical neurons, immune cell lineages) and more distant species.

In conclusion, by enabling unsupervised, interpretable, and biologically grounded cell-type correspondence, OT-MESH can advance the field’s ability to trace the evolution of cellular diversity and specialization across species, offering a valuable tool for comparative genomics and evolutionary biology.

References

- [1] Jingjing Wang, Huiyu Sun, Mengmeng Jiang, Jiaqi Li, Peijing Zhang, Haide Chen, Yuqing Mei, Lijiang Fei, Shujing Lai, Xiaoping Han, Xinhui Song, Suhong Xu, Ming Chen, Hongwei Ouyang, Dan Zhang, Guo-Cheng Yuan, and Guoji Guo. Tracing cell-type evolution by cross-species comparison of cell atlases. *Cell Reports*, 34(9):108803, March 2021.
- [2] Joshua Hahn, Aboozar Monavarfeshani, Mu Qiao, Allison H. Kao, Yvonne Kölsch, Ayush Kumar, Vincent P. Kunze, Ashley M. Rasys, Rose Richardson, Joseph B. Wekselblatt, Herwig Baier, Robert J. Lucas, Wei Li, Markus Meister, Joshua T. Trachtenberg, Wenjun Yan, Yi-Rong Peng, Joshua R. Sanes, and Karthik Shekhar. Evolution of neuronal cell classes and types in the vertebrate retina. *Nature*, 624(7991):415–424, December 2023.
- [3] Maxwell E. R. Shafer. Cross-Species Analysis of Single-Cell Transcriptomic Data. *Front. Cell Dev. Biol.*, 7, September 2019.
- [4] Karthik Shekhar, Sylvain W. Lapan, Irene E. Whitney, Nicholas M. Tran, Evan Z. Macosko, Monika Kowalczyk, Xian Adiconis, Joshua Z. Levin, James Nemeshegyi, Melissa Goldman, Steven A. McCarroll, Constance L. Cepko, Aviv Regev, and Joshua R. Sanes. COMPREHENSIVE CLASSIFICATION OF RETINAL BIPOLAR NEURONS BY SINGLE-CELL TRANSCRIPTOMICS. *Cell*, 166(5):1308–1323.e30, August 2016.
- [5] Yi-Rong Peng, Karthik Shekhar, Wenjun Yan, Dustin Herrmann, Anna Sappington, Gregory S. Bryman, Tavé van Zyl, Michael Tri H. Do, Aviv Regev, and Joshua R. Sanes. Molecular Classification and Comparative Taxonomics of Foveal and Peripheral Cells in Primate Retina. *Cell*, 176(5):1222–1237.e22, February 2019.
- [6] Lin Zhang, Martina Cavallini, Junqiang Wang, Ruiqi Xin, Qiangge Zhang, Guoping Feng, Joshua R. Sanes, and Yi-Rong Peng. Evolutionary and developmental specialization of foveal cell types in the marmoset. *Proc Natl Acad Sci U S A*, 121(16):e2313820121, April 2024.

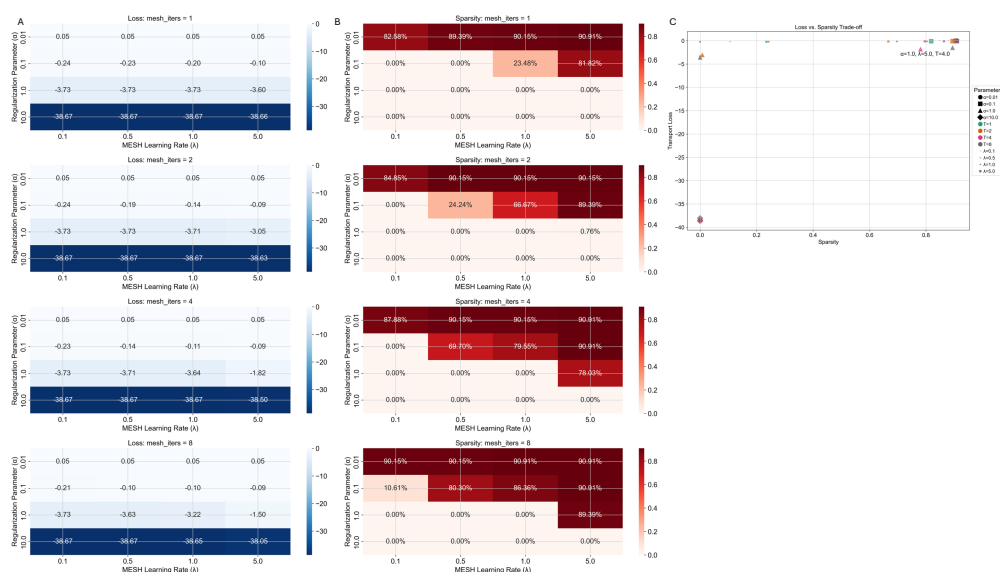
- [7] Junqiang Wang, Lin Zhang, Martina Cavallini, Ali Pahlevan, Junwei Sun, Ala Morshedian, Gordon L. Fain, Alapakkam P. Sampath, and Yi-Rong Peng. Molecular characterization of the sea lamprey retina illuminates the evolutionary origin of retinal cell types. *Nat Commun*, 15(1):10761, December 2024.
- [8] Andrew Butler, Paul Hoffman, Peter Smibert, Efthymia Papalexi, and Rahul Satija. Integrating single-cell transcriptomic data across different conditions, technologies, and species. *Nat Biotechnol*, 36(5):411–420, May 2018.
- [9] Ilya Korsunsky, Nghia Millard, Jean Fan, Kamil Slowikowski, Fan Zhang, Kevin Wei, Yuriy Baglaenko, Michael Brenner, Po-ru Loh, and Soumya Raychaudhuri. Fast, sensitive and accurate integration of single-cell data with Harmony. *Nat Methods*, 16(12):1289–1296, December 2019.
- [10] Yanay Rosen, Maria Brbić, Yusuf Roohani, Kyle Swanson, Ziang Li, and Jure Leskovec. Toward universal cell embeddings: Integrating single-cell RNA-seq datasets across species with SATURN. *Nat Methods*, 21(8):1492–1500, August 2024.
- [11] Tom Baden. The vertebrate retina: A window into the evolution of computation in the brain. *Current Opinion in Behavioral Sciences*, 57:101391, June 2024.
- [12] Yan Zhang, David W. Zhang, Simon Lacoste-Julien, Gertjan J. Burghouts, and Cees G. M. Snoek. Unlocking Slot Attention by Changing Optimal Transport Costs, May 2023. Comment: Published at International Conference on Machine Learning (ICML) 2023.
- [13] Francesco Locatello, Dirk Weissenborn, Thomas Unterthiner, Aravindh Mahendran, Georg Heigold, Jakob Uszkoreit, Alexey Dosovitskiy, and Thomas Kipf. Object-Centric Learning with Slot Attention, October 2020. Comment: NeurIPS 2020. Code available at https://github.com/google-research/google-research/tree/master/slot_attention.
- [14] Michael E. Sander, Pierre Ablin, Mathieu Blondel, and Gabriel Peyré. Sinkformers: Transformers with Doubly Stochastic Attention. In *Proceedings of The 25th International Conference on Artificial Intelligence and Statistics*, pages 3515–3530. PMLR, May 2022.
- [15] Nicholas M. Tran, Karthik Shekhar, Irene E. Whitney, Anne Jacobi, Inbal Benhar, Guosong Hong, Wenjun Yan, Xian Adiconis, McKinzie E. Arnold, Jung Min Lee, Joshua Z. Levin, Dingchang Lin, Chen Wang, Charles M. Lieber, Aviv Regev, Zhigang He, and Joshua R. Sanes. Single-cell profiles of retinal neurons differing in resilience to injury reveal neuroprotective genes. *bioRxiv*, page 711762, July 2019.
- [16] Anna Y. M. Wang, Manoj M. Kulkarni, Amanda J. McLaughlin, Jacqueline Gayet, Benjamin E. Smith, Max Hauptschein, Cyrus F. McHugh, Yvette Y. Yao, and Teresa Puthussery. An ON-type direction-selective ganglion cell in primate retina. *Nature*, 623(7986):381–386, November 2023.
- [17] Marco Cuturi. Sinkhorn Distances: Lightspeed Computation of Optimal Transportation Distances, June 2013.
- [18] Pinar Demetci, Rebecca Santorella, Björn Sandstede, William Stafford Noble, and Ritambhara Singh. SCOT: Single-Cell Multi-Omics Alignment with Optimal Transport. *J Comput Biol*, 29(1):3–18, January 2022.
- [19] Federico Gossi, Pushpak Pati, Panagiotis Chouvardas, Adriano Luca Martinelli, Marianna Kruithof-de Julio, and Maria Anna Rapsomaniki. Matching single cells across modalities with contrastive learning and optimal transport. *Briefings in Bioinformatics*, 24(3):bbad130, May 2023.
- [20] Sebastian Pena, Lin Lin, and Jia Li. Constructing Cell-type Taxonomy by Optimal Transport with Relaxed Marginal Constraints. *arXiv:2501.18650*, January 2025.
- [21] Mu Qiao. Factorized discriminant analysis for genetic signatures of neuronal phenotypes. *Front. Neuroinform.*, 17, December 2023.
- [22] Mu Qiao. Deciphering the genetic code of neuronal type connectivity through bilinear modeling. *Elife*, 12:RP91532, June 2024.

- [23] Jillian Goetz, Zachary F. Jessen, Anne Jacobi, Adam Mani, Sam Cooler, Devon Greer, Sabah Kadri, Jeremy Segal, Karthik Shekhar, Joshua R. Sanes, and Gregory W. Schwartz. Unified classification of mouse retinal ganglion cells using function, morphology, and gene expression. *Cell Rep*, 40(2):111040, July 2022.
- [24] Thomas Euler, Silke Haverkamp, Timm Schubert, and Tom Baden. Retinal bipolar cells: Elementary building blocks of vision. *Nature Reviews Neuroscience*, 15(8):507–519, August 2014.
- [25] Yoshihiko Tsukamoto and Naoko Omi. ON Bipolar Cells in Macaque Retina: Type-Specific Synaptic Connectivity with Special Reference to OFF Counterparts. *Front. Neuroanat.*, 10, October 2016.

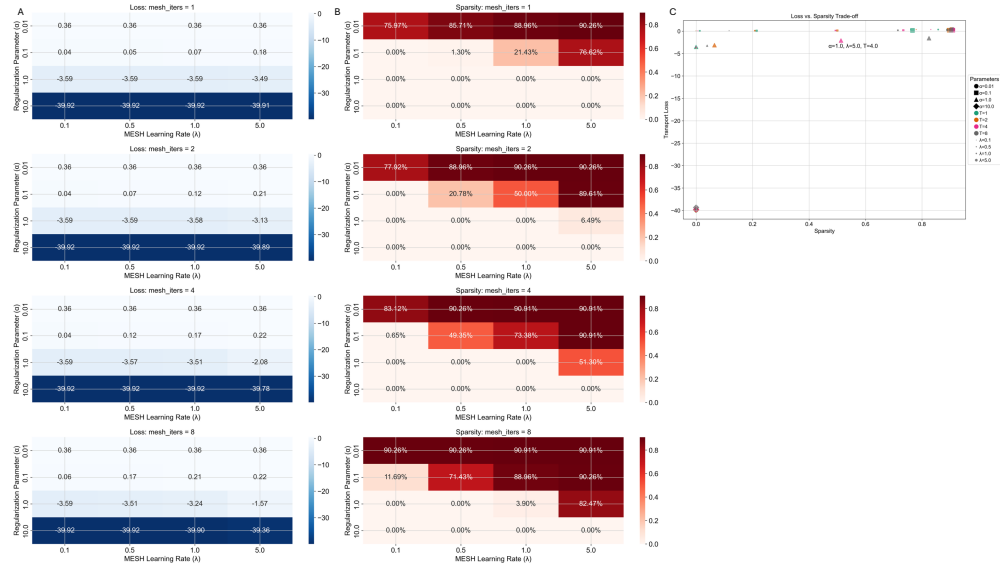
7 Data and Code Availability

All datasets used in this study are publicly available and cited in the manuscript. The code implementing the described OT-MESH framework for evolutionary cell type matching is available at <https://github.com/muqiao0626/Evo-Cell-Type-OT-MESH>. All experiments used Python 3.10.12 and runtime measurements were done on Apple M1 Max with 64GB RAM.

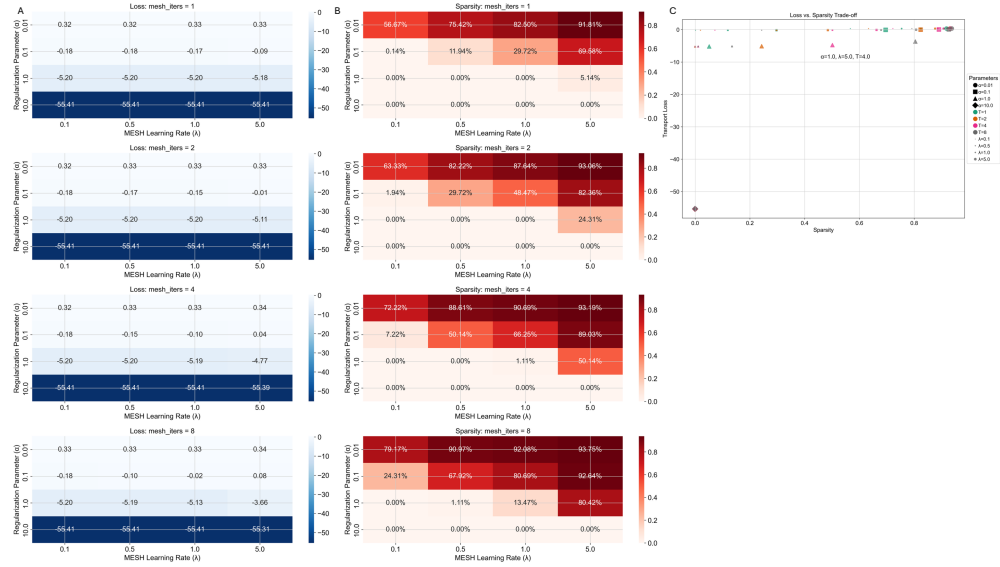
8 Supplementary Materials



Supplementary Figure 1: Parameter optimization of OT-MESH for the correspondence between macaque peripheral and foveal BC types. A) Transport loss across parameter combinations, with regularization parameter (α) on vertical axis and MESH learning rate (λ) on horizontal axis. Each subpanel shows results for different MESH iteration counts (T). B) Sparseness scores for the same parameter combinations, showing the percentage of near-zero (< 0.001) entries in the correspondence matrix. C) Trade-off between transport loss and sparseness across all parameter combinations. Each point represents a parameter set (shape/color/size coded as indicated in the legend). The optimal parameter set ($\alpha = 1.0, \lambda = 5.0, T = 4$) is labeled in the plot.



Supplementary Figure 2: Parameter optimization of OT-MESH for cross-species BC type correspondence. A) Transport loss across parameter combinations, with regularization parameter (α) on vertical axis and MESH learning rate (λ) on horizontal axis. Each subpanel shows results for different MESH iteration counts (T). B) Sparseness scores for the same parameter combinations, showing the percentage of near-zero (< 0.001) entries in the correspondence matrix. C) Trade-off between transport loss and sparseness across all parameter combinations. Each point represents a parameter set (shape/color/size coded as indicated in the legend). The optimal parameter set ($\alpha = 1.0, \lambda = 5.0, T = 4$) is labeled in the plot.



Supplementary Figure 3: Parameter optimization of OT-MESH for cross-species RGC type correspondence. A) Transport loss across parameter combinations, with regularization parameter (α) on vertical axis and MESH learning rate (λ) on horizontal axis. Each subpanel shows results for different MESH iteration counts (T). B) Sparseness scores for the same parameter combinations, showing the percentage of near-zero (< 0.001) entries in the correspondence matrix. C) Trade-off between transport loss and sparseness across all parameter combinations. Each point represents a parameter set (shape/color/size coded as indicated in the legend). The optimal parameter set ($\alpha = 1.0, \lambda = 5.0, T = 4$) is labeled in the plot.

Supplementary Table 1: Top-ranked correspondences between macaque and mouse BC types quantified by alignment scores (Eq.16).

Macaque BC Types (Peng et al. 2019)	Mouse BC Types (Shekhar et al. 2016)	Alignment Score
RB	RBC	0.9101
DB3a	BC3A	0.8930
DB1	BC2	0.8731
DB2	BC4	0.8458
IMB	BC7	0.8277
DB3b	BC3B	0.8268
DB6	BC6	0.8172
BB/GB*	BC8/9	0.7330
DB4	BC5D	0.6630
DB5*	BC5B	0.6496
FMB	BC1A	0.6261
DB5*	BC5C	0.4649
DB4	BC5A	0.4108
FMB	BC1B	0.4015

Supplementary Table 2: Top 10 correspondences between macaque and mouse RGC types quantified by alignment scores. Mouse RGC annotations from Tran et al. [15] and Goetz et al. [23].

Macaque RGC (Peng et al. 2019)	Mouse RGC (Tran et al. 2019)	Mouse RGC Annotation	Alignment Score
fRGC12	C10	ON direction-selective	0.6616
PG_OFF	C45	OFF transient alpha	0.6060
fRGC14	C40	M1 ipRGC	0.5967
MG_ON	C43	ON sustained alpha	0.5242
fRGC5	C8		0.4058
fRGC14	C33	M1 ipRGC	0.3971
PG_OFF	C34		0.3524
PG_ON	C41	ON transient alpha	0.2345
fRGC11	C3	F-mini-ON	0.2156
MG_OFF	C42	OFF sustained alpha	0.1995